NMRlipids III: Lipid–Cholesterol Interactions in Atomistic Molecular Dynamics Simulations

Fernando Favela-Rosales,[†] Peter Heftberger,[‡] Matti Javanainen,[*,¶,§] Jesper J. Madsen,[‖,⊥] Josef Melcr,[¶] Markus Miettinen,[#] O. H. Samuli Ollila,[*,¶,§] Georg Pabst,[‡,@] and Thomas Piggot[△,∇]

†*Departamento de Física, Centro de Investigación y de Estudios Avanzados del IPN, Apartado Postal 14-740, 07000 México D.F., México*

‡*Institute of Molecular Biosciences, Biophysics Division, NAWI Graz, University of Graz, Graz 8010, Austria*

¶*Institute of Organic Chemistry and Biochemistry, Academy of Sciences of the Czech Republic, Prague 6, Czech Republic*

§*Institute of Biotechnology, University of Helsinki*

‖*Department of Global Health, College of Public Health*

⊥*University of South Florida*

#*MPI*

@*BioTechMed-Graz, Graz 8010, Austria*

△*School of Chemistry, University of Southamptaon, Southampton SO17 1BJ, United Kingdom*

∇*Chemical Biological and Radiological Sciences, Defence Science and Technology Laboratory, Porton Down, Salisbury, Wiltshire SP4 0JQ, United Kingdom*

E-mail: matti.javanainen@helsinki.fi; samuli.ollila@helsinki.fi

1.Update Author list & Affiliations

Abstract

Cholesterol is a central building block in biomembranes, where it induces orientational order, slows down diffusion, and thereby renders the membrane stiffer. Molecular dynamics simulations have played a crucial role in resolving these effects and the underlying molecular picture, yet it has recently become evident that different simulation models predict quantitatively different behavior. Such limitations are easily neglected, as the field rapidly progresses towards simulations of complex membranes mimicking the *in vivo* conditions. Still, for their validity, it is crucial that the interactions between the fundamental building blocks of biomembranes, such as phospholipids and cholesterol, are modelled accurately. Here, we perform a systematic comparison of the ability of commonly used force fields to describe the structure and dynamics of binary mixtures of phosphatidylcholine and cholesterol. Comparison of lipid bilayer simulations with deuterium order parameters and lateral diffusion coefficients from NMR as well as form factors from X-ray scattering reveals that none of the existing force field outperforms the others across the physiologically relevant cholesterol concentrations. The Amber-compatible force fields show the smallest deviations from experiment with Slipids and Lipid17 models excelling at low and high cholesterol concentrations, respectively. The accompanied X-ray scattering data set measured for this work will foster future force field development and refinement.

1 Introduction

2.Check that the uses of "model" and "force field" are consistent

Cellular membranes contain an incredibly complex mixture of lipid molecules[1] which are unevenly distributed in the membrane plane and across its leaflets.[2–4] A key player driving the lateral heterogeneity is cholesterol (CHOL), which is present at concentrations between ∼10 mol-% (endoplasmic reticulum) and up to ∼50 mol-% (plasma membrane).[2] CHOL has the unique ability to order neighbouring lipids and thus induce the liquid ordered (L_o) phase in model membranes.[5–8] In the cellular setting, the interaction between phospholipids and

CHOL is associated with the formation of lipid rafts and nanodomains.[9,10] This heterogeneity can then further regulate protein distribution[11] or conformation,[12] in addition to the direct modulation of protein function.[13,14]

While the structure and dynamics of heterogeneous membranes are difficult to capture experimentally, atomistic resolution molecular dynamics (MD) simulations are widely used to provide a detailed view of complex membranes and the lateral organization of lipid bilayers driven by lipid–CHOL interactions.[8,15–18] This is further facilitated by an increasing selection of available force fields with compatible lipid and protein parameters that enable the simulations of ever more complex and realistic membranes .

The traditional protein force fields CHARMM,[19] AMBER,[20] and OPLS[21,22] now have growing libraries of compatible lipid molecules, including CHOL, in the forms of CHARMM36,[23,24] Lipid17/Slipids,[25–30] and the model by Maciejewski and Rog (here "MacRog"),[31–34] respectively. Notably, simulations using CHARMM36, Lipid17, and Slipids are now readily set up using CHARMM-GUI for multiple simulation engines that enables rapid set up of complex membrane simulations.[35,36]

While simulating of complex membranes with cholesterol have become relatively straightforward task, estimating the trustworthiness of MD simulations for complex membranes remains a challenge. Our earlier work has demonstrated that the conformational ensembles of lipids from an MD simulation can be evaluated against C-H bond order parameters from solid state NMR experiments.[37–41] This approach has been useful for finding the best models for headgroups of phosphatidylcholine (PC),[37] phosphatidylserine (PS),[40] phoshatidylethanolamine (PE)[41] and phosphatidylglycerol (PG) lipids,[41] for evaluating and improving membrane interactions with ions[39–43] and small molecules,[44] and for finding simulation parameters predicting most realistic packing properties of membranes.[45,46] Furthermore, quantitative quality measures based on C-H bond order parameters have been recently defined and used to rank simulations in the NMRlipids databank.[46] However, such automatic quality evaluation is limited to simulations that have experimental data available with cor-

responding composition and temperature. Because simulations mimicking all experimental compositions for multi-component membranes are often tedious to produce, quality evaluation of mixed lipid bilayers is not yet fully automized in the NMRlipids databank.

Here, we demonstrate how simulations of binary POPC-cholesterol mixtures can be evaluated against experimental NMR and X-ray scattering data by interpolating through multiple CHOL concentrations. Because effect of cholesterol on lipid headgroup and its decoupling of acyl chain ordering has been discussed previously,[37,47] we focus here on acyl chains that are expected to play larger role in cholesterol induced lateral membrane heterogeneity. We also evaluated the dependence of lateral diffusion coefficients on cholesterol against pulsed field gradient (PFG) NMR experiments[48,49] using the recent theoretical work that allows a quantitative comparison with experiment after eliminating the finite-size effects in MD simulations.[50,51] With the structural and dynamic comparisons established, we estimated the quality of popular force fields at different CHOL concentrations. We then used the best-performing force fields to analyze molecular organization at different cholesterol concentrations, as we expect them to best reflect this organization in reality. While we focus here on POPC-cholesterol mixture, we expect our results to set guidelines for future efforts to validate intermolecular interactions in binary and more complex systems.

2 Methods

2.1 X-ray Scattering Experiments

Fully hydrated multilamellar vesicles (MLVs), composed of POPC and CHOL with the latter present at 0–50 mol-% with 5 mol-% increments, were prepared for small angle X-ray scattering (SAXS) experiments using rapid solvent exchange as described previously[52,53] . This avoids the precipitation of cholesterol crystallites at high concentration[54] yielding non-phase separated samples up to 50 mol-% cholesterol content. Lipids, purchased from Avanti Polar Lipids (Alabaster, AL, USA), were used as dry powders without any further purification.

All other chemicals were obtained in pro analysis quality from Lactan (Graz, Austria). The data were obtained at the EMBL BioSAXS beamline (Hamburg) using 20 keV photons at $T = 300$ K and analyzed in terms of the SDP-GAP model described in Refs. 55 and 56. The data from MLVs contain the structure factor (the crystalline lattice) and form factor in a convoluted fashion, yet by fitting the scattered intensity data we obtained both contributions. The electron density profiles were modelled from form factors using the SDP model where volume distribution functions are modelled by individual Gaussians or error functions.[57–59] Cholesterol was described using two Gaussians, as proposed by Jianjun Pan (private communication), and used in Refs. 53 and 60. Membrane thickness was defined as twice the distance from the electron density maximum to the membrane center. The electron density maxima were extracted by the `findpeaks` function in Matlab after smoothening the electron density data.

2.2 Molecular Dynamics Simulations

We performed MD simulations of a pure POPC membrane as well as five POPC/CHOL mixtures with CHOL content ranging from 11 to 47 mol-%. Systems were simulated using four commonly used force fields, namely CHARMM36,[23,24] Amber-compatible Slipids[27–29] with its 2020 update,[30] Amber-compatible Lipid17,[25,26] and OPLS-aa-compatible MacRog[32–34] models. In order to eliminate the finite size effects due to periodic boundary conditions from lateral diffusion coefficients of lipids, we performed all simulations in three sizes (64, 256 or 1024 POPC molecules). The number of POPC molecules was kept constant across the different CHOL concentrations. All membranes were solvated by 50 waters per lipid (POPC or CHOL). All simulations were 1 µs long, totaling 72 µs, and performed using GROMACS version 2020 or 2021.[61] The used simulation parameters are provided in Table S1, and the simulation data are available at DOI: 10.5281/zenodo.7035350 (CHARMM36), DOI: 10.5281/zenodo.7022749 (Slipids), DOI: 10.5281/zenodo.6992065 (Lipid17), and DOI: 10.5281/zenodo.7061800 (MacRog). All simulations were stored to the NMRlipids databank[46] with the ID numbers

listed in Table S2.

3.Run Lipid21 for revision?

Table 1: Details of the simulation systems provided for (small/medium/large) system sizes). The box dimensions in the membrane plane (x/y) and normal to the membrane (z) are provided for the Slipids simulations, and the values vary slightly between the force fields.

[CHOL]	POPC	CHOL	Water	x/y (nm)	z (nm)
0 mol-%	64/256/1024	0/0/0	3200/12800/51200	4.4/9.0/18.1	8.9/8.6/8.5
11 mol-%	64/256/1024	8/32/128	3600/14400/57600	4.5/9.4/18.1	9.4/9.1/9.3
20 mol-%	64/256/1024	16/64/256	4000/16000/64000	4.5/9.2/18.3	10.2/9.9/10.0
29 mol-%	64/256/1024	26/104/416	4500/18000/72000	4.6/9.2/18.5	10.8/10.8/10.7
38 mol-%	64/256/1024	40/160/640	5200/20800/83200	4.8/9.5/19.2	11.3/11.4/11.2
47 mol-%	64/256/1024	56/224/896	6000/24000/96000	5.0/10.1/20.0	11.8/11.6/11.7

2.3 Simulation Analyses

Structural properties: The C–H bond order parameters, form factors and electron density profiles automatically calculated by the NMRlipids Databank[46] were used. Similarly to the experimental X-ray scattering data, membrane thickness was defined as twice the distance from the electron density maximum to the membrane center. Locations of maxima were extracted by the `findpeaks` function in Matlab after smoothening the electron density data. Area per phospholipid was obtained by dividing the area of the bilayer by the number of phospholipids in one leaflet. To simplify the interpolation, C-H bond order parameters of 2 (3) hydrogens in CH_2 (CH_3) groups in the POPC acyl chains were averaged. These groups rotate freely and thus the order parameters are essentially identical for both (all) hydrogens in experiments and simulations. An exception to this are the hydrogens bound to the 2nd carbon in the oleate chain; they lack rotational averaging in both both simulations and experiments, and were thus treated separately in our analyses. The C–H order parameters for the POPC head group are shown separately for all CH_2 groups, *i.e.* no averaging was performed.

Lateral Diffusion Coefficients: The lateral diffusion coefficients D_{PBC} from simulations performed using periodic boundary conditions (PBC) were extracted from mean squared displacement (MSD) data calculated for lipid centers of mass after eliminating the drift of their host leaflet with the `gmx msd` tool. The MSD data were fit with a straight line in the lag time (Δ) interval between 10 and 100 ns as

$$\mathrm{MSD} = 4D_{\mathrm{PBC}}\Delta. \tag{1}$$

The diffusion coefficients extracted from the three simulation box sizes were fitted with

$$D_{\mathrm{PBC}} \approx D_{\infty} + \frac{k_{\mathrm{B}}T}{4\pi\mu_{\mathrm{m}}h}\frac{\ln\left[L/\left(L_{\mathrm{SD}}+1.565H\right)\right]-1.713}{1+H/L_{\mathrm{SD}}}, \tag{2}$$

where D_{∞} is the lateral diffusion coefficient in an infinite system, h is the hydrodynamic thickness of the membrane, $k_{\mathrm{B}}T$ is the Boltzmann constant, T is the temperature, H is half the thickness of the water layer, $L_{\mathrm{SD}} = \frac{h\mu_{\mathrm{m}}}{2\mu_{\mathrm{f}}}$ the Saffmann–Delbrück length, and μ_{m} and μ_{f} are shear viscosities of the membrane and the fluid (water), respectively.[51] The inter-leaflet friction coefficient does not appear in Eq. (2) as we expect it to be infinite, which was found to be a valid assumption for lipid bilayers.[51] The water viscosity value of 0.3228 mPa·s was interpolated to 298 K from the values for CHARMM TIP3P in Ref. 62 and used for all simulations (CHARMM TIP3P and normal TIP3P differ by ∼2–3%). The final simulation box dimensions were used for L and H. For h and H ($= (L_z - h)/2$, the average values from the three systems sizes were used.

Quantitative Quality evaluation of cholesterol effect on membrane properties: To ease the evaluation of simulations against experimental data with non-matching concentrations, we interpolated the effect of cholesterol in simulations and experiments for cholesterol concentrations ranging from 0% to 50%. Continuous 2D matrices were created by interpolation for the oleate and palmitate chain order parameters (as a function of carbon

atoms in the acyl chains) and the electron density profiles (as a function of normal distance from bilayer center), while 1D interpolation was used for the cholesterol dependence of the 1st and 2nd form factor minima locations, and diffusion coefficients. These interpolations were then used to calculate deviations (in %) from experimental values across CHOL concentrations to quantify the quality of the lipid force fields. For the 2D matrices, the absolute values of the differences between matrices from simulations and experiments were first calculated. The averages of differences over the carbon atoms in the acyl chain (order parameters) or across the simulation system (density profiles) were then calculated. This resulted in 1D deviation vectors as a function of CHOL concentration. For diffusion coefficients and form factor minima, the absolute value of the difference of the interpolated 1D vectors of simulation and experimental data was calculated to provide deviation as a function of CHOL concentration. All these 1D vectors were normalized by dividing them by the experimental values to provide relative deviations in % between a simulation and experiments as a function of cholesterol concentration. For C-H bond order parameters, also the deviation matrices between simulations and experiments were used to illustrate quality of simulations.

More and Less Ordered Populations: The angles (θ) between the C–H vectors of the last six carbons of the palmitate chain were extracted and the data across all CHOL concentrations was accumulated. These data were fit with two Gaussians centered at 0,

$$P(\theta) = a_{\text{less}} \exp\left(-\frac{\theta}{2\sigma_{\text{less}}}\right) + a_{\text{more}} \exp\left(-\frac{\theta}{2\sigma_{\text{more}}}\right), \tag{3}$$

where the two standard deviations (σ) correspond to the more and less ordered components. After these σ values were established for a given force field, the data at all CHOL concentrations were independently fitted by Eq. (3) with the fixed σ values. These fits provided the pre-factors, whose ratio $a_{\text{more}}/(a_{\text{more}} + a_{\text{less}})$ corresponds to the fraction of the more ordered component in the system.

This two-Gaussian approach assumes a "two-population" scheme, where the more and less

ordered populations are present (at non-zero CHOL concentration), and that the addition of CHOL only affects their ratio, but not their natures. In an alternative picture of a "collective transition", there would be a single Gaussian, whose standard deviation σ would decrease as a function of CHOL concentration as the membrane gets more ordered.

3 Results and Discussion

4.Results: volmaps of chains around cholesterol?

5.Results: SI: RDFs of POPC chains and CHOL around CHOL

6.Unify colours in figures

3.1 Acyl Chain Ordering Varies Greatly Between the Force Fields

Cholesterol is known to induce order in cell membranes by increasing the fraction of *anti* conformations in the acyl chains of phospholipids,[63] which is suggested to play critical role in the phase behaviour of PC–cholesterol mixtures.[6] Consequently, the correct cholesterol ordering effect is expected to be a necessary condition for a model used to understand lipid–cholesterol phase behaviour. Cholesterol ordering effect can be experimentally quantified by measuring the C-H bond order parameters using ^{13}C or ^{2}H NMR techniques that can be also directly compared with MD simulations.[38] Simulations generally reproduce the cholesterol ordering effect, but order parameters often deviate from experiments at high cholesterol concentrations.[26,63] Furthermore, it has not been clear how accurately different force field parameters capture the details of lipid-cholesterol interactions and which parameters would give most realistic results for simulations of complex mixtures where such interactions play critical roles.

Here, we evaluate the cholesterol ordering effect in state of the art force field parameters against C-H bond order parameter data from ^{13}C NMR experiments measured from POPC-

cholesterol mixture with cholesterol concentratons ranging between 0-60%.[63] To this end, we first interpolated order parameter maps as a function of acyl chain carbon number and cholesterol concentration for both simulations and experiments. These maps were then subtracted to obtain the deviation maps between simulations and experiments. The deviation maps of different force fields are shown for the palmitate (top row) and oleate (bottom row) chains of POPC in Fig. 1, whereas the original order parameter profiles are shown in Figs. S6 and S7.

The cholesterol ordering effect is manifested in original profiles in Figs. S6 and S7 as substantial increase in absolute values of acyl chain C–H bond order parameters upon addition of cholesterol in all simulation models and experiments. The deviations mapped in Fig. 1 provide an intuitive view for a quantitative comparison of different force fields with experiments. In white regions, the simulation results are considered to fall within the experimental error as the deviations are in the range of [–0.02,0.02]. Blue indicates that the order parameters are too negative, i.e., the acyl chains are too ordered in simulations, and *vice versa* for red. Overall, the simulation models behave reasonably well at low CHOL concentrations, but deviate significantly from experiment at higher CHOL concentrations.

In CHARMM36, the both the palmitate and oleate chains get too ordered upon increasing CHOL concentration, yet the oleate C9 carbon next to the double bond is too disordered in the simulation. The oleate chain shows best agreement with experiment in Slipids with only slight excess ordering at higher CHOL concentrations. The excess ordering is more severe for the palmitate chain. Still, the major discrepancy between Slipids and experiment is the drastically too disordered C2 and C3 carbons of the palmitate chain. This effect was not present in the original Slipids model,[46] indicating that it was introduced in the recent reparametrization that improved the head group and glycerol backbone structures of Slipids.[30] Lipid17 provides the best overall agreement with experiment, as no segments deviate significantly from experiment at any CHOL concentrations. At low CHOL concentrations, the middle of the oleate chain is too disordered. At large CHOL concentrations,

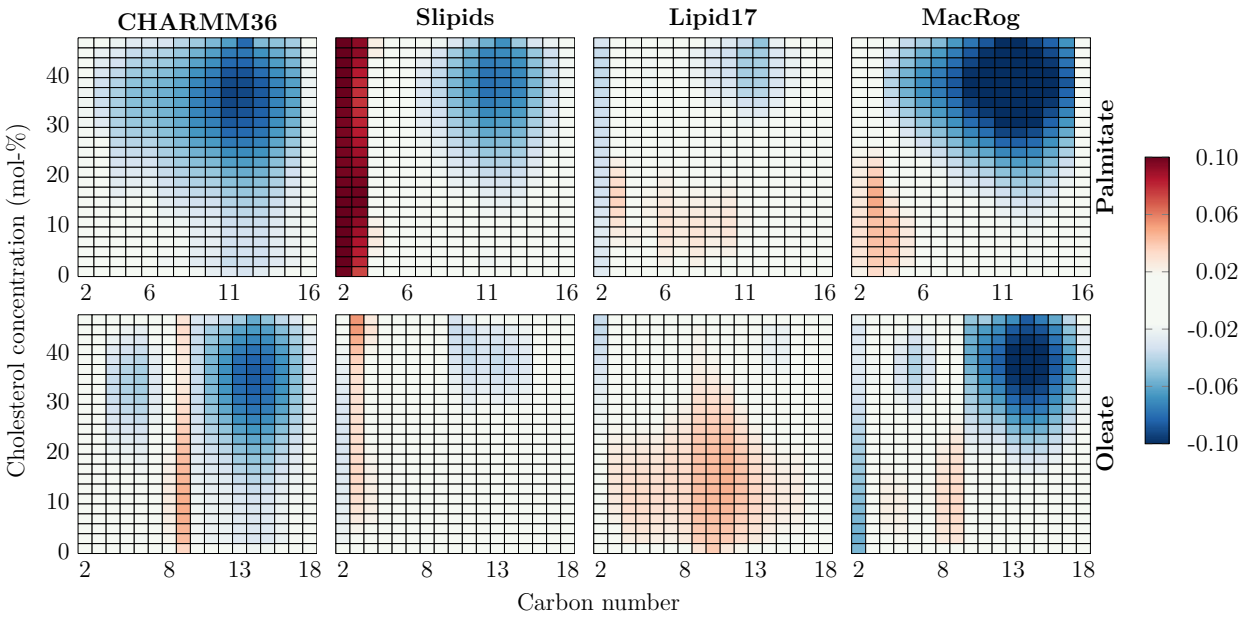

Figure 1: POPC acyl chain order parameter deviation from experiments. Data are shown for palmitate (top row) and oleate (bottom row) and for the four force fields (columns). Negative values indicate that order is too high ($-S_{\mathrm{CH}}$ values too negative) in the simulations. The values that are within the estimated experimental error range of 0.02[38] are coloured in white. Order parameters of identical hydrogens attached to the same carbons were averaged with the exception of C2 carbon of the oleate chain with the forked order parameters for which differences for both the larger and smaller values were calculated, and the average of this deviation is shown in the C2 column of oleate.

the oleate chain agrees well with experiment, whereas the palmitate chain has a slightly too ordered C9–C12 segment, yet the deviation is significantly smaller than in the other force fields. MacRog behaves reasonably well at low CHOL concentrations, yet the C2–C5 carbons in palmitate are slightly too disordered, whereas the C2 of oleate is somewhat too ordered. However, at larger CHOL concentrations the chains become overall way too ordered, leading to the largest overall deviations from experiment.

7.Cholesterol order parameters? Into the deviation metric?

3.2 Cholesterol Effect on membrane properties is Manifested Differently in Different Force Fields

Cholesterol induced ordering straigthens the acyl chain conformations that leads to thickening of membranes. While acyl chain order and membrane thickness are well correlated,[46] lipid bilayer dimensions can be accessed more directly by measuring X-ray scattering form factor, which is related to the electron density along membrane normal *via* a Fourier transform.[38,56,64,65] Electron density profile, area per lipid and bilayer thickness can be extracted from the form factor using the scattering density profile (SDP) model or its combination with MD simulations.[56,58,64–66] To complement the evaluation of cholesterol ordering effect against NMR order parameters, we measured also X-ray scattering form factors from POPC-cholesterol mixtures with systematically increasing cholesterol concentrations. Scattering intensitities from experiments are shown in Figs. S1 and S2, form factors from experiments and simulations in Fig. S3, and density profiles in Fig. S5.

While the absolute and relative lobe amplitudes depend on simulation box size, minima in form factors correlate with membrane dimensions.[46] Thus, we interpolated the locations of first two minima in the form factors to the entire studied range of CHOL concentrations in Fig. S4. The plots in Fig. S4 highlight that the addition of CHOL first shifts the first minima to smaller wave vector values in the experiment, which is reasonably well captured by the simulation force fields. CHARMM36 seems to be off more than the other three force fields. Above ∼25 mol-% of CHOL, the location of the minimum shifts to larger wave vector values in the experiment, which is curiously not captured by any of the force fields. The experiment shows a steady shift of the second minimum to smaller wave vector values, and this is reproduced by all simulation force fields. Slipids and Lipid17 are generally in better agreement with the experiment than MacRog and CHARMM36.

Effect of cholesterol on structural properties of bilayers is compared between the SDP model (based on experimental form factors) and MD simulation results in Fig. 2. All models demonstrate increasing thickness upon addition of cholesterol that saturates after approxi-

mately 30 mol-% (bottom middle panel in Fig. 2). MD simulations agree well with the SDP model below 30 mol-% but overshoot the SDP results at high cholesterol concentrations. Lipid17 simulations are exception as they predict thinner membranes than SDP model at low cholesterol concentrations, and clear saturation of thickness increase is not observed. The dependence of APL on CHOL concentration follows the trends in thickness inversely in general (bottom right panel of Fig. 2), yet provide curious differences between the force fields at the physiologically relevant CHOL concentration range.[2] Lipid17 has the largest APL across the entire CHOL contration range. MacRog also has a large APL for pure POPC, but the partial area of CHOL is negative until 30 mol-% concentration indicating a particularly strong condensation effect. The profiles for Slipids and CHARMM36 are very similar with the small or zero cholesterol partial area until a concentration of 20 mol-%.

For more detailed comparison of membrane structure, we interpolated the changes in electron density profiles along membrane normal (Fig. S5) as a function of cholesterol concentration to create two-dimensional electron density maps shown in Fig. 2. Overall, all electron density profiles share the same features across all CHOL concentrations; a high-density band corresponding to the tightly-packed interfacial region containing electron-rich phoshorus, a low-density region at the core of the membrane occupied by the disordered acyl chains, and intermediate density in the rest of the lipid regions as well as the aqueous phase. However, a more detailed look at the profiles in Fig. 2 reveals differences between the force fields. Fig. 2 also demonstrates that CHARMM36 has the sharpest low- and high-density bands indicating smaller membrane fluctuations that would smear the bands, and the same is true for MacRog at higher cholesterol concentrations. The less sharp bands for Lipid17 and especially Slipids profiles indicate that the membranes are more flexible with these force fields.

Comparison against experiments (bottom left panel in Fig. 2) indicates that the membrane structure is more uniform in the experiment, as the bands are sharper. This is also evident in the original electron density profiles in Fig. S5. System size plays a role here,

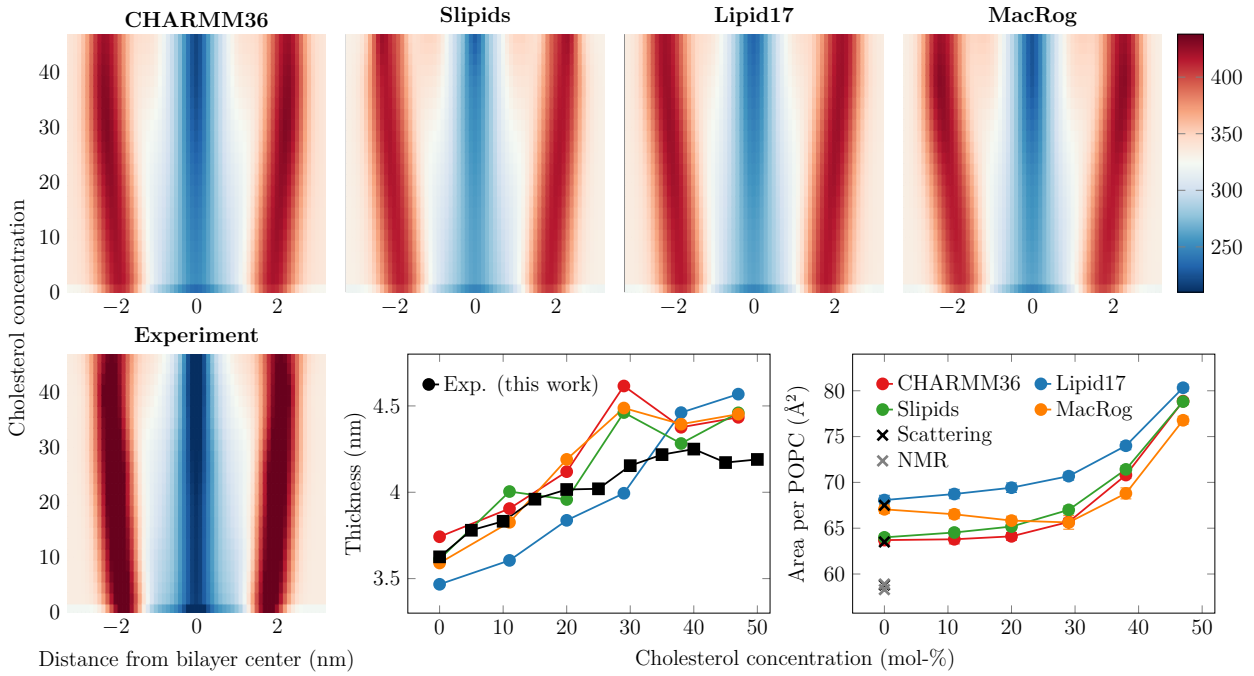

Figure 2: **Electron density profiles, thickness and area per lipid as a function of CHOL concentration.** Top: Electron density maps for the simulations using four different force fields. Bottom left: Electron density map for the experiment. The scaling is uniform between all simulations and experiment. The original electron density profiles are shown in Fig. S5. The effect of system size on the density profiles in simulations is demonstrated in Fig. S12 in the SI. Bottom center: Bilayer thickness. Thickness is defined as twice the distance from the peak in electron density to the membrane core. Experimental data are extracted in a similar manner from electron density profiles obtained with X-ray scattering. Bottom right: area per lipid measured by dividing the total membrane area by the number of phospholipids. The experimental estimates, interpolated to 298 K, are taken from Refs. 67 (58.8 Å^2), 68 (67.5 Å^2), and 69 (63.5 Å^2). The NMR data is measured in Ref. 70 using either ^{13}C (58.9 Å^2) or ^{2}H (58.3 Å^2) NMR. The size-dependency of area per lipid is shown in Fig. S11.

as demonstrated by the density maps calculated for the CHARMM36 simulations in three sizes, shown in Fig. S12. The larger the system, the larger the bilayer undulations are, which can smear the features of the density profiles. Still, even in the smallest system, the band intensities are not as localized as in the experiment. This difference likely partially stems from the features of the used SDP model, but it could also indicate different elastic properties between simulation and experiment.

3.3 The Force Fields Predict Very Different Lateral Mobilities

Apart from the ordering effect on the bilayer structure, CHOL is also known to make them stiffer and less dynamic.[8,48,49] The comparison between lateral diffusion coefficients extracted from simulation and experiment has been limited due to a box-size dependence observed in simulations performed using periodic boundary conditions.[50,51,71] Here, we tackle this issue by performing simulations with three system sizes, which allows the extrapolation of the results to an infinite system with the theoretical description developed by Vögele and Hummer.[51,51] The size-dependence of lipid lateral diffusion from simulations together with the fit of Eq. (2) are shown in Fig. S9, whereas the CHOL-dependence of these values in systems with different sizes are shown in Fig. S10. The PBC-corrected lateral diffusion coefficients are shown in the top panel of Fig. 3 together with experimental values from ^{1}H pulsed field gradient NMR diffusion measurements on label-free macroscopically aligned bilayers.[48,49]

The lipid models again show significantly different behavior. CHARMM36 and Lipid17 provide drastically too large diffusion coefficients at low CHOL concentrations, yet they converge towards experimental estimates upon the addition of CHOL. This similar behavior is somewhat surprising, as they behave very differently in terms of both area per POPC (Fig. 2) and acyl chain ordering (Fig. 1). For CHARMM36, the excessive ordering observed at high CHOL concentrations counterbalances the too fast dynamics observed at low CHOL concentrations. However, the behavior of Lipid17 cannot be explained by the order parameters, as they agree with experiment relatively well across all studied CHOL concentrations. The area per POPC is exaggerated at all CHOL concentrations, yet the deviation from experiment decreases towards larger CHOL concentrations. Thus, it seems that CHARMM36 dynamics correlate with chain ordering, whereas those of Lipid17 go hand in hand with area per POPC. With MacRog, the dynamics of POPC are already slightly too slow compared to experiment, and the excessive ordering at large CHOL concentrations leads to a larger underestimation of the experimental values. Curiously, Slipids provides an essentially quantitative agreement with experiment across the studied CHOL concentrations, and thus significantly outperforms

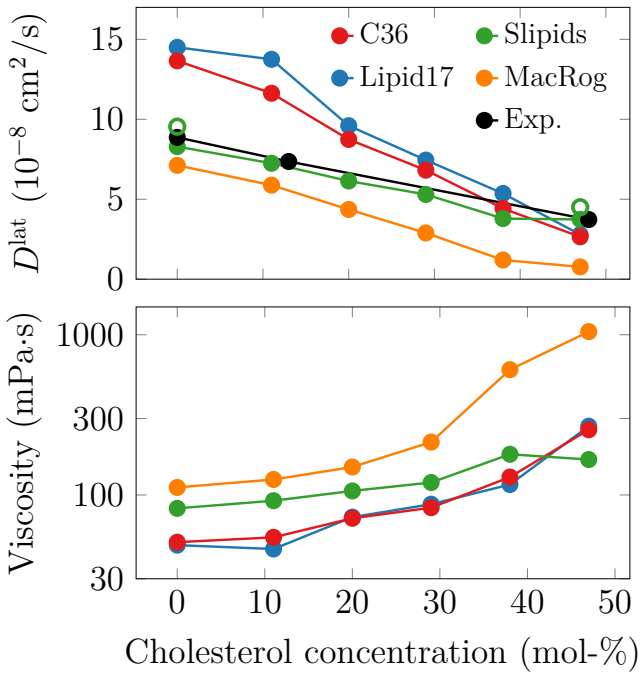

Figure 3: **Dynamic properties of the POPC/cholesterol mixtures.** Top: Lateral diffusion coefficients corrected for finite-size effects using Eq. (**??**). Experimental data are taken from NMR measurements on well-hydrated samples.[48,49] The hollow circles show data extracted for Slipids using a shorter Lennard-Jones cutoff (see text). Bottom: Shear viscosities obtained from the finite-size correction. Eq. (**??**). The size-dependence of lateral diffusion and the fits used to obtain the PBC-corrected diffusion coefficients and shear viscosities are shown in Figs. S9 and S10.

other force fields in terms of lateral dynamics.

Slipids has the largest Lennard-Jones (LJ) cutoff of the used force fields of 1.4 nm (see Table S1), and this cutoff is known to affect dynamic properties.[72] Therefore, we repeated simulations at 0 mol-% and 47 mol-% CHOL for Slipids but with a cutoff of 0.9 nm corresponding to that of Lipid17, and the PBC-corrected diffusion coefficient values are shown in the top panel of Fig. 3 as hollow green circles. The decrease in cutoff indeed leads to a minor increase in the lateral diffusion coefficient. However, the LJ cutoff alone does not explain the differences between force fields, indicating that they truly spark from differences in the force field interaction parameters.

As the results in Fig. S10 demonstrate, the PBC correction can qualitatively change the trends observed for diffusion coefficients. This results from the fact that the size of the PBC

correction, Eq. (2), depends on membrane viscosity, which further depends on CHOL concentration. For example, Lipid17 and CHARMM36 underestimate the experimental values in all system sizes used here and the effect of CHOL seems to be well reproduced. However, the corrected values significantly overshoot the experiment at low CHOL concentration, and CHOL induces a more drastic slowdown in simulations so that the simulations and experiment almost agree at 47 mol-% CHOL. With MacRog, even the corrected values fall below the experimental ones, yet the slowdown effect of CHOL again seems stronger than in experiment. Slipids is a clear outlier, as the CHOL-dependence seems too weak with finite system sizes, yet after accounting for PBC effects, the agreement with experiment is excellent. These results highlight that little can be said about CHOL-dependence of lateral diffusion coefficients without performing multiple simulations required for the PBC correction at multiple CHOL concentrations. When fine-tuning interaction parameters, this can lead to a massive number of simulations.

The PBC correction, Eq. (2) also provides the shear viscosity of the membrane as a fitting parameter. Instead of shear viscosity, the surface viscosity is sometimes reported, yet this is simply the product of shear viscosity and membrane thickness (available in Fig. 2). The shear viscosity values are in line with the lateral diffusion coefficients.

3.4 Quality of Force Fields at Various Cholesterol Concentrations

The previous sections reveal differences in predictions of force fields for the effect of cholesterol on membrane properties. To streamline the selection of force fields that best capture the effect of cholesterol on different membrane properties, we used the interpolated data to calculate the relative deviations from experiments (difference of simulated and experimental values divided by the experimental value) for the form factor minima, the order parameters of the two acyl chains, and the diffusion coefficients from all the force fields.

The deviations in Fig. 4 reveals that Slipids provides overall the best agreement with experiment, yet its quality decreases slightly at higher CHOL concentrations. Lipid17 pro-

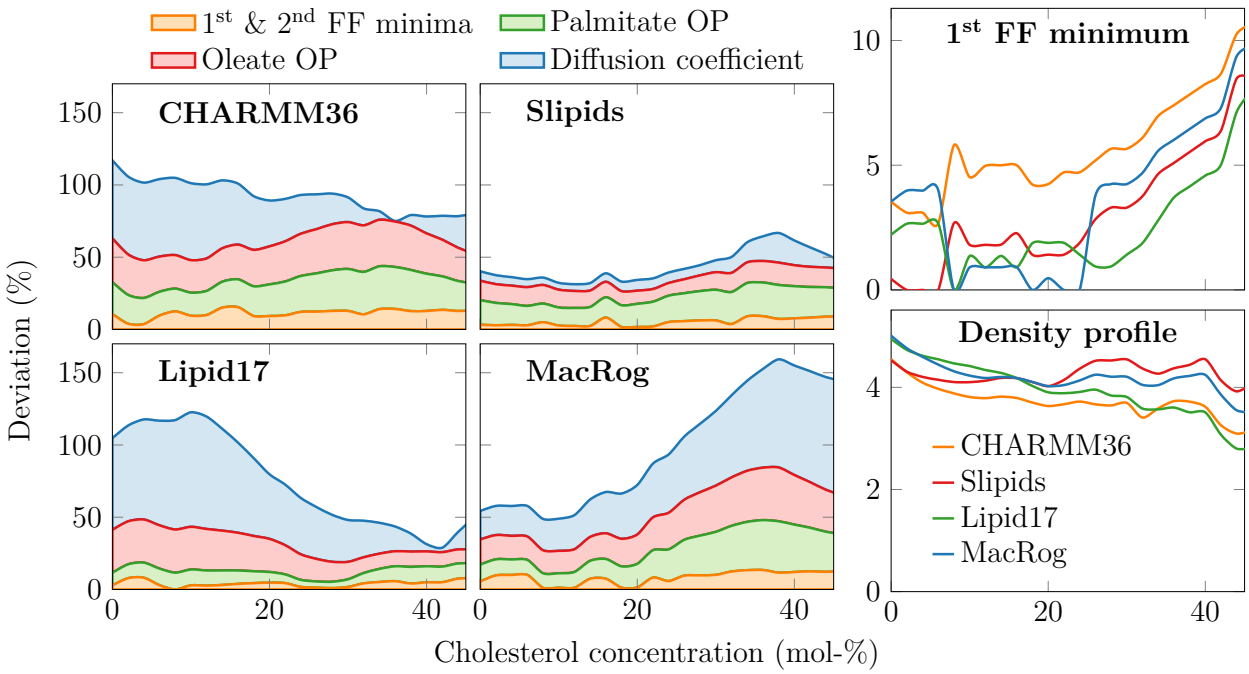

Figure 4: **Total deviation of the force fields from experimental data.** Two leftmost columns: The relative deviations from the first two minima in the form factor, palmitate and oleate chain order parameters, and diffusion coefficients are shown in a cumulative manner to highlight the overall deviation of the force fields from experimental data. The order parameter deviations are obtained by averaging over the columns in Fig. 1 and normalizing against experimental data. The differences in the form factor minima in Fig. **??** between experiment and simulation were calculated, normalized against experimental data, and summed together. The diffusion coefficient deviation is the difference of values from simulation and experiment in Fig. 3, taken after interpolation to the same CHOL values as shown in Figs. 1 and 2, and normalized against experimental values. Top right panel: The zoomed-in view to the deviation in the location of the first minimum in the form factor. Bottom right panel: Deviation of the density profiles calculated from the form factor using the SDS model. The density profile deviations are calculated as the difference between the simulation and experimental maps in Fig. 2 followed by averaging over the columns and normalization against experiment.

vides slightly better agreement with experiment above ∼30 mol-% of CHOL than Slipids, but exhibits major deviation from experiments with low cholesterol concentrations. MacRog performs relatively well at low CHOL concentrations, but its quality deteriorates significantly upon the addition of CHOL. The deviation metric for CHARMM36 are significant with all cholesterol concentrations. Since the contributions from the form factor minima deviations are barely visible for some force fields in the leftmost columns of Fig. 4, we have

highlighted the error in the 1st minimum location in the top right panel of Fig. 4. This panel demonstrates that apart from CHARMM36, all force fields capture the location of the 1st minimum relatively well at low CHOL concentrations, but deviate significantly at larger CHOL concentrations.

Finally, we also analyzed the deviations in the density profiles in the bottom right panel of Fig. 4. This analysis demonstrates that even the significant deviations as well as the trend as a function of CHOL concentration in the form factor minima are lost as form factors are converted to density profiles. This indicates that the form factor minima are a better target value for force field development and refinement.

3.5 Cholesterol Induces Order in a Non-collective Manner

CHOL could induce order in a lipid membrane in two ways; it could either increase the average order of all phospholipids ("collective transition"), or increase the prevalence of the ordered lipids ("two state model"). To clarify this effect, we extracted the C–H angle distributions with respect to the xy plane for the last six carbons of the palmitate chain from all force fields. We first accumulated data at all CHOL concentrations, and observed that these data could be fitted with two Gaussian functions. These Gaussians were centered at 0°, and with the different standard deviations they corresponding to the more and less ordered acyl chains. The obtained standard deviations for the more and less ordered chains only showed minor differences between the force fields (rightmost panel in Fig. 5). We then fitted the C–H angle distributions for all CHOL concentrations with the two Gaussians with the obtained standard deviations and with their means set to 0. These Gaussians provided provided excellent fits to the data with $R^2 = 0.991 \pm 0.005$ (see the leftmost panel of Fig. 5 for the fits to the Slipids data). The prefactors of the Gaussian functions were considered to represent the fractions of the more and less ordered components in the system. In pure POPC, the ordered component was absent, yet its prevalence increased linearly as a function of CHOL, after saturating at high CHOL concentrations (rightmost panel in Fig. 5). The

success of the two-Gaussian fits in describing the data indicates that with all force fields the bilayer is composed of lipids ordered by CHOL and lipids corresponding to their state in pure POPC membrane, *i.e.* corresponding to the "two state model", and CHOL simply changes the fraction of these two states present. Indeed, single Gaussian fits with the standard deviation as a free parameter fail when CHOL is present, indicating that the ordering does not occur *via* a "collective transition".

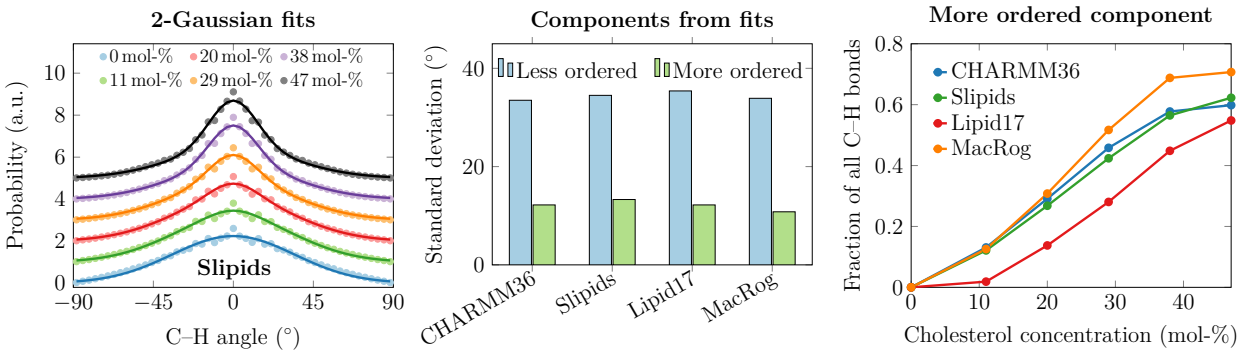

Figure 5: **Distributions of C–H bond orientations.** Leftmost panel: The probability distributions for the angle of C–H vectors of the last 6 carbons in the palmitate chain of POPC with respect to the xy-plane. All distributions are centered around 0, but have different shapes. The markers show data extracted from Slipids simulations at various CHOL concentrations, and the solid lines show two-Gaussian fits with fixed standard deviations to the data. These Gaussians correspond to the more and less ordered palmitate chains. The fixed standard deviations were extracted from a fit of two Gaussians to the data accumulated across all CHOL concentrations. The fit with the fixed standard deviations to all CHOL concentrations are excellent with $R^2 = 0.991 \pm 0.005$ (mean $\pm$ standard deviation). Middle panel: The standard deviations of the two Gaussians fitted to the C–H distribution (such as the one in the leftmost panel) for the four force fields. Rightmost panel: The fraction of the more ordered component as a function of CHOL concentration extracted simply by dividing the prefactor in the Gaussian distribution for the more ordered component by the sum of the two prefactors. Notably, in the CHOL-free system, the ordered component is not present.

3.6 Molecular Level Structure of PC–CHOL Mixtures

Molecular dynamics simulations provide a description of the molecular organization of POPC and CHOL in the bilayer, yet the reliability of this description depends on the quality of the used force field. In the previous section we established that Slipids and Lipid17 provide the best agreement with experimental properties at low and high CHOL concentrations,

respectively. Thus, it is reasonable to assume that the molecular pictures provided by these two force fields at the corresponding CHOL concentration regimes are the most realistic.

Earlier studies have analyzed the organization of CHOL and DSPC chains and observed five and three density peaks for DSPC chains and other CHOL molecules around CHOL molecules.[73]

2D density maps RDFs to SI?

Apart from the lateral organization of the molecules, their orientations might also differ between the force fields. However, we observed only small differences in the tilt of CHOL molecules, defined by the angle between a vector spanning the rigid ring structure as well as the z axis (membrane lies in the x, y plane). The mean angles and their standard deviations are shown in Fig. S13. Lipid17 and Slipids show very consistent values. CHARMM36 has slightly smaller tilt angles than them across all CHOL concentrations. MacRog has the most tilted CHOL molecules at low CHOL concentrations, but their tilt angle is the smallest at large CHOL concentrations. Still, the differences are overall minor.

4 Conclusions

The tested all-atom force fields captured the most important general effects of cholesterol on membrane properties: increased acyl chain ordering, concomitant increase in bilayer thickness, and reduced lateral diffusion rate of lipids. However, quantitative comparison reveals differences between force fields and their qualities evaluated against NMR and X-ray scattering data. Comparison with NMR order parameters and X-ray scattering form factors propose that simulations reproduce experimental results up to 20 mol-% of cholesterol, but overestimate acyl chain ordering and membrane thickness after further addition of cholesterol. Apparent exception to this are Lipid17 simulations, yet their seemingly better agreement with experiments can be explained by underestimated acyl chain order with low cholesterol concentrations that approaches experiments upon addition of cholesterol and finally over-

shoots the experimental results. In conclusion, unified picture emerging from comparison with NMR and X-ray scattering data suggests that all the tested force fields overestimate the cholesterol ordering effect, particularly above 20 mol-% of cholesterol. Previously published comparison[63] suggests the same conclusion for historically relevant Berger/Höltje force field parameters that were not included in this work.

Besides the ordering effect, effect of cholesterol on membrane properties has been discussed also in terms of the cholesterol condensing effect which refers to a decrease in the *area per phospholipid* upon the addition of cholesterol (negative partial area),[74] or to CHOL having a diminishing partial area, meaning that a certain amount of CHOL could be added to a phospholipid bilayer without effecting its total area (zero partial area).[75] At the physiological CHOL concentrations in the range from 0 to 30 mol-%, only MacRog predicts negative partial area for cholesterol, while CHARMM36 predicts zero partial area, and Slipids and Lipid17 predict small positive partial area. Considering that Slipids and Lipid17 perform best in our quality evaluation against experiments, yet still slightly overestimating the cholesterol condensing effect, our results suggests that cholesterol has positive but small partial area.

Considering also lateral dynamics, Slipids is overall closest to experiments among the parameters tested here, and is therefore probably the best choice for studies where lipid-cholesterol interactions play major role. Nevertheless, all tested parameters capture qualitative effects of cholesterol on membrane properties relatively well and differences between force fields are clearly smaller than, for example, in the case of PC-PS lipid mixtures.[45] Therefore, quality of selected force field for other molecules, such as, other lipids, proteins, sugars, or drugs, together with force field compatibility might be more relevant decisive factor for simulations of complex systems. Finally, it must be noted that while all simulations were performed with their suggested simulation parameters, the different simulation engines might provide slightly different behavior, yet we believe that evaluating the magnitude of these effects is well beyond the scope of this work.

Our results demonstrate that quality evaluation of lipid mixture simulations against ex-

perimental NMR and X-ray scattering data give consistent results for how accurately force field parameters capture intermolecular interactions. The interpolation approach introduced here extends the NMRlipids databank quality metrics[46] beyond individual systems enabling automatic ranking of not only lipid mixtures but also membrane mixed with other molecules such as ions. Such tools will strongly support the emerging endeavours for automatic improvements of force field parameters.[45]

Supporting Information Available

Simulation parameters used for all the studied force fields. Form factor plots from simulations and experiments with the traced minima at various cholesterol concentrations. Interpolated 1st and 2nd minima of the form factors as a function of cholesterol concentration from simulation and experiment. Electron density profiles from simulation and experiment at various cholesterol concentrations. Deuterium order parameters of both acyl chains of POPC from simulation and experiment at various cholesterol concentrations. Deviation of POPC head group order parameters from experiment as a function of cholesterol concentration. Lateral diffusion coefficients with varying cholesterol concentrations as a function of simulation box size from simulations together with the extrapolation of these values to an infinite box size. Diffusion coefficients as a function of cholesterol concentration from simulations with varying box sizes together with comparison to experiment. Effect of simulation box size on the area per lipid across the studied cholesterol concentrations. Effect of simulation box size on the density profiles across the studied cholesterol concentrations. Cholesterol tilt as a function of cholesterol concentration from simulations.

Acknowledgement

We acknowledge CSC – IT Center for Science for computational resources. JJM thanks the Amber community (Benjamin Madej from the Walker lab and Callum Dickson from the

Gould lab) for technical assistance related to the lipid14 force field parameters. MJ thanks the Academy of Finland (Postdoctoral researcher grant no. 338160) and the Emil Aaltonen foundation for funding.

References

(1) Lorent, J.; Levental, K.; Ganesan, L.; Rivera-Longsworth, G.; Sezgin, E.; Doktorova, M.; Lyman, E.; Levental, I. Plasma membranes are asymmetric in lipid unsaturation, packing and protein shape. *Nature chemical biology* **2020**, *16*, 644–652.

(2) Van Meer, G.; Voelker, D. R.; Feigenson, G. W. Membrane lipids: where they are and how they behave. *Nature reviews Molecular cell biology* **2008**, *9*, 112–124.

(3) Wang, H.-Y.; Bharti, D.; Levental, I. Membrane heterogeneity beyond the plasma membrane. *Frontiers in Cell and Developmental Biology* **2020**, *8*, 580814.

(4) Kinnun, J. J.; Bolmatov, D.; Lavrentovich, M. O.; Katsaras, J. Lateral heterogeneity and domain formation in cellular membranes. *Chemistry and Physics of Lipids* **2020**, *232*, 104976.

(5) Mouritsen, O. G.; Zuckermann, M. J. What's so special about cholesterol? *Lipids* **2004**, *39*, 1101–1113.

(6) Ipsen, J. H.; Karlström, G.; Mouritsen, O.; Wennerström, H.; Zuckermann, M. Phase equilibria in the phosphatidylcholine-cholesterol system. *Biochim. Biophys. Acta* **1987**, *905*, 162 – 172.

(7) Kinnunen, P. K. On the principles of functional ordering in biological membranes. *Chemistry and Physics of Lipids* **1991**, *57*, 375 – 399.

(8) Róg, T.; Pasenkiewicz-Gierula, M.; Vattulainen, I.; Karttunen, M. Ordering effects

of cholesterol and its analogues. *Biochimica et Biophysica Acta (BBA)-Biomembranes* **2009**, *1788*, 97–121.

(9) Simons, K.; Ikonen, E. Functional rafts in cell membranes. *Nature* **1997**, *387*, 569–572.

(10) Cebecauer, M.; Amaro, M.; Jurkiewicz, P.; Sarmento, M. J.; Sachl, R.; Cwiklik, L.; Hof, M. Membrane lipid nanodomains. *Chemical reviews* **2018**, *118*, 11259–11297.

(11) Milovanovic, D.; Honigmann, A.; Koike, S.; Göttfert, F.; Pähler, G.; Junius, M.; Müllar, S.; Diederichsen, U.; Janshoff, A.; Grubmüller, H.; Eggeling, C.; Hell, S. W.; van den Bogaart, G.; Jahn, R. Hydrophobic mismatch sorts SNARE proteins into distinct membrane domains. *Nature Communications* **2015**, *6*, 1–10.

(12) Kelkar, D. A.; Chattopadhyay, A. Modulation of gramicidin channel conformation and organization by hydrophobic mismatch in saturated phosphatidylcholine bilayers. *Biochimica et Biophysica Acta (BBA)–Biomembranes* **2007**, *1768*, 1103–1113.

(13) Gimpl, G. Interaction of G protein coupled receptors and cholesterol. *Chemistry and physics of lipids* **2016**, *199*, 61–73.

(14) Guixà-González, R.; Albasanz, J. L.; Rodriguez-Espigares, I.; Pastor, M.; Sanz, F.; Martí-Solano, M.; Manna, M.; Martinez-Seara, H.; Hildebrand, P. W.; Martín, M.; Selent, J. Membrane cholesterol access into a G-protein-coupled receptor. *Nature Communications* **2017**, *8*, 1–12.

(15) Róg, T.; Vattulainen, I. Cholesterol, sphingolipids, and glycolipids: What do we know about their role in raft-like membranes? *Chem. Phys. Lipids* **2014**, *184*, 82 – 104.

(16) Berkowitz, M. L. Detailed molecular dynamics simulations of model biological membranes containing cholesterol. *Biochimica et Biophysica Acta (BBA)-Biomembranes* **2009**, *1788*, 86–96.

(17) Enkavi, G.; Javanainen, M.; Kulig, W.; Róg, T.; Vattulainen, I. Multiscale simulations of biological membranes: the challenge to understand biological phenomena in a living substance. *Chemical reviews* **2019**, *119*, 5607–5774.

(18) Marrink, S. J.; Corradi, V.; Souza, P. C.; Ingolfsson, H. I.; Tieleman, D. P.; Sansom, M. S. Computational Modeling of Realistic Cell Membranes. *Chemical Reviews* **2019**, *119*, 6184–6226.

(19) Brooks, B. R.; Bruccoleri, R. E.; Olafson, B. D.; States, D. J.; Swaminathan, S. a.; Karplus, M. CHARMM: a program for macromolecular energy, minimization, and dynamics calculations. *Journal of computational chemistry* **1983**, *4*, 187–217.

(20) Cornell, W. D.; Cieplak, P.; Bayly, C. I.; Gould, I. R.; Merz, K. M.; Ferguson, D. M.; Spellmeyer, D. C.; Fox, T.; Caldwell, J. W.; Kollman, P. A. A second generation force field for the simulation of proteins, nucleic acids, and organic molecules. *Journal of the American Chemical Society* **1995**, *117*, 5179–5197.

(21) Jorgensen, W. L.; Tirado-Rives, J. The OPLS force field for proteins. Energy minimizations for crystals of cyclic peptides and crambin. *J. Am. Chem. Soc* **1988**, *110*, 1657–1666.

(22) Harder, E.; Damm, W.; Maple, J.; Wu, C.; Reboul, M.; Xiang, J. Y.; Wang, L.; Lupyan, D.; Dahlgren, M. K.; Knight, J. L., et al. OPLS3: a force field providing broad coverage of drug-like small molecules and proteins. *Journal of chemical theory and computation* **2016**, *12*, 281–296.

(23) Klauda, J. B.; Kučerka, N.; Brooks, B. R.; Pastor, R. W.; Nagle, J. F. Simulation-Based Methods for Interpreting X-Ray Data from Lipid Bilayers. *Biophys. J.* **2006**, *90*, 2796 – 2807.

(24) Lim, J. B.; Rogaski, B.; Klauda, J. B. Update of the Cholesterol Force Field Parameters in CHARMM. *J. Phys. Chem. B* **2012**, *116*, 203–210.

(25) Dickson, C. J.; Madej, B. D.; Skjevik, A. A.; Betz, R. M.; Teigen, K.; Gould, I. R.; Walker, R. C. Lipid14: The Amber Lipid Force Field. *J. Chem. Theory Comput.* **2014**, *10*, 865–879.

(26) Madej, B. D.; Gould, I. R.; Walker, R. C. A Parameterization of Cholesterol for Mixed Lipid Bilayer Simulation within the Amber Lipid14 Force Field. *J. Phys. Chem. B* **2015**, *119*, 12424–12435.

(27) Jämbeck, J. P. M.; Lyubartsev, A. P. Derivation and Systematic Validation of a Refined All-Atom Force Field for Phosphatidylcholine Lipids. *J. Phys. Chem. B* **2012**, *116*, 3164–3179.

(28) Jämbeck, J. P. M.; Lyubartsev, A. P. An Extension and Further Validation of an All-Atomistic Force Field for Biological Membranes. *J. Chem. Theory Comput.* **2012**, *8*, 2938–2948.

(29) Jämbeck, J. P. M.; Lyubartsev, A. P. Another Piece of the Membrane Puzzle: Extending Slipids Further. *Journal of Chemical Theory and Computation* **2013**, *9*, 774–784.

(30) Grote, F.; Lyubartsev, A. P. Optimization of slipids force field parameters describing headgroups of phospholipids. *The Journal of Physical Chemistry B* **2020**, *124*, 8784–8793.

(31) Maciejewski, A.; Pasenkiewicz-Gierula, M.; Cramariuc, O.; Vattulainen, I.; Róg, T. Refined OPLS All-Atom Force Field for Saturated Phosphatidylcholine Bilayers at Full Hydration. *J. Phys. Chem. B* **2014**, *118*, 4571–4581.

(32) Kulig, W.; Tynkkynen, J.; Javanainen, M.; Manna, M.; Róg, T.; Vattulainen, I.; Jungwirth, P. How well does cholesteryl hemisuccinate mimic cholesterol in saturated phospholipid bilayers? *Journal of Molecular Modeling* **2014**, *20*.

(33) Kulig, W.; Jurkiewicz, P.; Olżyńska, A.; Tynkkynen, J.; Javanainen, M.; Manna, M.; Róg, T.; Hof, M.; Vattulainen, I.; Jungwirth, P. Experimental determination and computational interpretation of biophysical properties of lipid bilayers enriched by cholesteryl hemisuccinate. *Biochim. Biophys. Acta* **2015**, *1848*, 422 – 432.

(34) Kulig, W.; Pasenkiewicz-Gierula, M.; Róg, T. Cis and trans unsaturated phosphatidylcholine bilayers: A molecular dynamics simulation study. *Chem. Phys. Lipids* **2016**, *195*, 12 – 20.

(35) Lee, J.; Cheng, X.; Swails, J. M.; Yeom, M. S.; Eastman, P. K.; Lemkul, J. A.; Wei, S.; Buckner, J.; Jeong, J. C.; Qi, Y.; Jo, S.; Pande, V. S.; Case, D. A.; Brooks, C. L.; MacKerell, A. D.; Klauda, J. B.; Im, W. CHARMM-GUI Input Generator for NAMD, GROMACS, AMBER, OpenMM, and CHARMM/OpenMM Simulations Using the CHARMM36 Additive Force Field. *Journal of Chemical Theory and Computation* **2016**, *12*, 405–413.

(36) Lee, J.; Hitzenberger, M.; Rieger, M.; Kern, N. R.; Zacharias, M.; Im, W. CHARMM-GUI supports the Amber force fields. *The Journal of chemical physics* **2020**, *153*, 035103.

(37) Botan, A.; Favela-Rosales, F.; Fuchs, P. F. J.; Javanainen, M.; Kanduč, M.; Kulig, W.; Lamberg, A.; Loison, C.; Lyubartsev, A.; Miettinen, M. S.; Monticelli, L.; Määttä, J.; Ollila, O. H. S.; Retegan, M.; Róg, T.; Santuz, H.; Tynkkynen, J. Toward Atomistic Resolution Structure of Phosphatidylcholine Headgroup and Glycerol Backbone at Different Ambient Conditions. *J. Phys. Chem. B* **2015**, *119*, 15075–15088.

(38) Ollila, O. S.; Pabst, G. Atomistic resolution structure and dynamics of lipid bilayers in simulations and experiments. *Biochimica et Biophysica Acta (BBA) - Biomembranes* **2016**, *1858*, 2512 – 2528, Biosimulations of lipid membranes coupled to experiments.

(39) Catte, A.; Girych, M.; Javanainen, M.; Loison, C.; Melcr, J.; Miettinen, M. S.; Mon-

ticelli, L.; Määttä, J.; Oganesyan, V. S.; Ollila, O. S., et al. Molecular electrometer and binding of cations to phospholipid bilayers. *Physical Chemistry Chemical Physics* **2016**, *18*, 32560–32569.

(40) Antila, H.; Buslaev, P.; Favela-Rosales, F.; Ferreira, T. M.; Gushchin, I.; Javanainen, M.; Kav, B.; Madsen, J. J.; Melcr, J.; Miettinen, M. S., et al. Headgroup structure and cation binding in phosphatidylserine lipid bilayers. *The Journal of Physical Chemistry B* **2019**, *123*, 9066–9079.

(41) Bacle, A.; Buslaev, P.; Garcia-Fandino, R.; Favela-Rosales, F.; Mendes Ferreira, T.; Fuchs, P. F.; Gushchin, I.; Javanainen, M.; Kiirikki, A. M.; Madsen, J. J., et al. Inverse conformational selection in lipid–protein binding. *Journal of the American Chemical Society* **2021**, *143*, 13701–13709.

(42) Melcr, J.; Martinez-Seara, H.; Nencini, R.; Kolafa, J.; Jungwirth, P.; Ollila, O. H. S. Accurate Binding of Sodium and Calcium to a POPC Bilayer by Effective Inclusion of Electronic Polarization. *J. Phys. Chem. B* **2018**, *122*, 4546–4557.

(43) Melcr, J.; Mendes Ferreira, T.; Jungwirth, P.; Ollila, O. S. Improved Cation Binding to Lipid Bilayer with Negatively Charged POPS by Effective Inclusion of Electronic Polarization. *J. Chem. Theory Comput.* **2019**, https://doi.org/10.1021/acs.jctc.9b00824.

(44) Nencini, R.; Ollila, O. H. S. Charged Small Molecule Binding to Membranes in MD Simulations Evaluated against NMR Experiments. *The Journal of Physical Chemistry B* **2022**, *126*, 6955–6963.

(45) Antila, H. S.; Kav, B.; Miettinen, M. S.; Martinez-Seara, H.; Jungwirth, P.; Ollila, O. S. Emerging Era of Biomolecular Membrane Simulations: Automated Physically-Justified Force Field Development and Quality-Evaluated Databanks. *The Journal of Physical Chemistry B* **2022**, *126*, 4169–4183.

(46) Kiirikki, A. M.; Antila, H. S.; Bort, L.; Buslaev, P.; Favela, F.; Ferreira, T. M.; Fuchs, P. F.; Garcia-Fandino, R.; Gushchin, I.; Kav, B.; Kula, P.; Kurki, M.; Kuzmin, A.; Madsen, J. J.; Miettinen, M. S.; Nencini, R.; Piggot, T.; Pineiro, A.; Samantray, S.; Suarez-Leston, F.; Ollila, O. H. S. NMRlipids Databank: Making data-driven analyses of membrane properties accessible for all. 2023; `https://doi.org/10.26434/chemrxiv-2023-jrpwm`.

(47) Antila, H. S.; Wurl, A.; Ollila, O. S.; Miettinen, M. S.; Ferreira, T. M. Rotational decoupling between the hydrophilic and hydrophobic regions in lipid membranes. *Biophysical Journal* **2022**, *121*, 68–78.

(48) Filippov, A.; Orädd, G.; Lindblom, G. The effect of cholesterol on the lateral diffusion of phospholipids in oriented bilayers. *Biophysical journal* **2003**, *84*, 3079–3086.

(49) Filippov, A.; Orädd, G.; Lindblom, G. Influence of cholesterol and water content on phospholipid lateral diffusion in bilayers. *Langmuir* **2003**, *19*, 6397–6400.

(50) Vögele, M.; Hummer, G. Divergent diffusion coefficients in simulations of fluids and lipid membranes. *The Journal of Physical Chemistry B* **2016**, *120*, 8722–8732.

(51) Vögele, M.; Köfinger, J.; Hummer, G. Hydrodynamics of diffusion in lipid membrane simulations. *Physical Review Letters* **2018**, *120*, 268104.

(52) Rieder, A.; Koller, D.; Lohner, K.; Pabst, G. Optimizing rapid solvent exchange preparation of multilamellar vesicles. *Chemistry and physics of lipids* **2015**, *186*, 39–44.

(53) Belička, M.; Weitzer, A.; Pabst, G. High-resolution structure of coexisting nanoscopic and microscopic lipid domains. *Soft Matter* **2017**, *13*, 1823–1833.

(54) Buboltz, J. T.; Feigenson, G. W. A novel strategy for the preparation of liposomes: rapid solvent exchange. *Biochimica et Biophysica Acta (BBA)-Biomembranes* **1999**, *1417*, 232–245.

(55) Heftberger, P.; Kollmitzer, B.; Heberle, F. A.; Pan, J.; Rappolt, M.; Amenitsch, H.; Kučerka, N.; Katsaras, J.; Pabst, G. Global small-angle X-ray scattering data analysis for multilamellar vesicles: the evolution of the scattering density profile model. *J. Appl. Crystallogr.* **2014**, *47*, 173–180.

(56) Heftberger, P.; Kollmitzer, B.; Rieder, A. A.; Amenitsch, H.; Pabst, G. In Situ Determination of Structure and Fluctuations of Coexisting Fluid Membrane Domains. *Biophys. J.* **2015**, *108*, 854 – 862.

(57) Heberle, F.; Pan, J.; Standaert, R.; Drazba, P.; Kučerka, N.; Katsaras, J. Model-based approaches for the determination of lipid bilayer structure from small-angle neutron and X-ray scattering data. *Eur. Biophys. J.* **2012**, *41*, 875–890.

(58) Kučerka, N.; Nagle, J. F.; Sachs, J. N.; Feller, S. E.; Pencer, J.; Jackson, A.; Katsaras, J. Lipid Bilayer Structure Determined by the Simultaneous Analysis of Neutron and X-Ray Scattering Data. *Biophys. J.* **2008**, *95*, 2356–2367.

(59) Kučerka, N.; Holland, B. W.; Gray, C. G.; Tomberli, B.; Katsaras, J. Scattering Density Profile Model of POPG Bilayers As Determined by Molecular Dynamics Simulations and Small-Angle Neutron and X-ray Scattering Experiments. *J. Phys. Chem. B* **2012**, *116*, 232–239.

(60) Heftberger, P. Structure and elasticity of fluid membrane domains. Ph.D. thesis, Graz University of Technology, 2015.

(61) Páll, S.; Zhmurov, A.; Bauer, P.; Abraham, M.; Lundborg, M.; Gray, A.; Hess, B.; Lindahl, E. Heterogeneous parallelization and acceleration of molecular dynamics simulations in GROMACS. *The Journal of Chemical Physics* **2020**, *153*, 134110.

(62) Ong, E. E.; Liow, J.-L. The temperature-dependent structure, hydrogen bonding and other related dynamic properties of the standard TIP3P and CHARMM-modified TIP3P water models. *Fluid Phase Equilibria* **2019**, *481*, 55–65.

(63) Ferreira, T. M.; Coreta-Gomes, F.; Ollila, O. H. S.; Moreno, M. J.; Vaz, W. L. C.; Topgaard, D. Cholesterol and POPC segmental order parameters in lipid membranes: solid state ^{1}H-^{13}C NMR and MD simulation studies. *Phys. Chem. Chem. Phys.* **2013**, *15*, 1976–1989.

(64) Pan, J.; Cheng, X.; Heberle, F. A.; Mostofian, B.; Kučerka, N.; Drazba, P.; Katsaras, J. Interactions between Ether Phospholipids and Cholesterol As Determined by Scattering and Molecular Dynamics Simulations. *J. Phys. Chem. B* **2012**, *116*, 14829–14838.

(65) Marquardt, D.; Heberle, F. A.; Nickels, J. D.; Pabst, G.; Katsaras, J. On scattered waves and lipid domains: detecting membrane rafts with X-rays and neutrons. *Soft Matter* **2015**, *11*, 9055–9072.

(66) Doktorova, M.; Kučerka, N.; Kinnun, J. J.; Pan, J.; Marquardt, D.; Scott, H. L.; Venable, R. M.; Pastor, R. W.; Wassall, S. R.; Katsaras, J.; Heberle, F. A. Molecular structure of sphingomyelin in fluid phase bilayers determined by the joint analysis of small-angle neutron and X-ray scattering data. *The Journal of Physical Chemistry B* **2020**, *124*, 5186–5200.

(67) Pabst, G.; Rappolt, M.; Amenitsch, H.; Laggner, P. Structural information from multilamellar liposomes at full hydration: full q-range fitting with high quality x-ray data. *Physical Review E* **2000**, *62*, 4000.

(68) Kučerka, N.; Tristram-Nagle, S.; Nagle, J. F. Structure of fully hydrated fluid phase lipid bilayers with monounsaturated chains. *The Journal of membrane biology* **2006**, *208*, 193–202.

(69) Kučerka, N.; Nieh, M. P.; Katsaras, J. Fluid phase lipid areas and bilayer thicknesses of commonly used phosphatidylcholines as a function of temperature. *Biochim. Biophys. Acta* **2011**, *1808*, 2761–2771.

(70) Leftin, A.; Molugu, T. R.; Job, C.; Beyer, K.; Brown, M. F. Area per Lipid and Cholesterol Interactions in Membranes from Separated Local-Field ^{13}C NMR Spectroscopy. *Biophys. J.* **2014**, *107*, 2274 – 2286.

(71) Camley, B. A.; Lerner, M. G.; Pastor, R. W.; Brown, F. L. Strong influence of periodic boundary conditions on lateral diffusion in lipid bilayer membranes. *The Journal of chemical physics* **2015**, *143*, 12B604_1.

(72) Leonard, A. N.; Simmonett, A. C.; Pickard IV, F. C.; Huang, J.; Venable, R. M.; Klauda, J. B.; Brooks, B. R.; Pastor, R. W. Comparison of additive and polarizable models with explicit treatment of long-range Lennard-Jones interactions using alkane simulations. *Journal of Chemical Theory and Computation* **2018**, *14*, 948–958.

(73) Martinez-Seara, H.; Róg, T.; Karttunen, M.; Vattulainen, I.; Reigada, R. Cholesterol induces specific spatial and orientational order in cholesterol/phospholipid membranes. *PloS one* **2010**, *5*, e11162.

(74) Edholm, O.; Nagle, J. F. Areas of molecules in membranes consisting of mixtures. *Biophysical journal* **2005**, *89*, 1827–1832.

(75) Javanainen, M.; Melcrová, A.; Magarkar, A.; Jurkiewicz, P.; Hof, M.; Jungwirth, P.; Martinez-Seara, H. Two cations, two mechanisms: interactions of sodium and calcium with zwitterionic lipid membranes. *Chemical Communications* **2017**, *53*, 5380–5383.

ToDo

P.